Optical downfolding method for calculating quasinormal modes of complex nanoparticles

Alexey A. Dmitriev [1,*] and Mikhail V. Rybin [1,2]
[1]*School of Physics and Engineering, ITMO University, St Petersburg 197101, Russia*
[2]*Ioffe Institute, St Petersburg 194021, Russia*

(Received 2 February 2021; accepted 12 April 2021; published 17 May 2021)

Optical oligomers are clusters consisting of several nanoparticles that support multipolar resonances. Each multipole couples to all multipoles in every other particle, leading to formation of a set of oligomer quasinormal modes. Here we present an "optical downfolding" method for semianalytical study of the optical oligomer quasinormal modes in the spectral region of the individual nanoparticle dipole resonance. We considered a dimer and a linear trimer of dielectric nanopillars for demonstration. Our studies revealed the physical nature of the Fabry-Pérot–like modes which manifest themselves as fringes in dimer scattering spectra at large separations between the particles. We have also demonstrated these modes to coalesce at an exceptional point. Finally, our studies uncovered which quasinormal modes interact resulting in the appearance of a Fano resonance in the scattering spectrum of a linear nanopillar trimer. Our results were verified by finite-element-method simulations.

DOI: 10.1103/PhysRevA.103.053514

I. INTRODUCTION

Metasurfaces are a versatile tool for light manipulation in nanoscale [1,2]. This is due to their ability to change the wavefront of an incident wave in the desired manner by resonant scattering on meta-atoms. This principle has been used in designing flat metalenses [3,4], structural colors [5], optical filters [6], vortex plates [7], and for many other applications. In order to realize all these devices, complex-shaped meta-atoms are used as structural elements. However, as their size must be much smaller than wavelength, they are mostly fabricated by costly techniques such as electron lithography and focused-ion-beam etching [8,9]. Photolithography has only limited application due to the light diffraction limit. These restrictions may be overcome by using laser ablation techniques [10] for producing drops of a simple shape. Still, it is possible to achieve a complex mode structure by organizing these drops into oligomers or metamolecules [11–19]. They support multiple quasinormal modes (QNMs), which are used to achieve complex scattering effects that involve several resonances.

In order to design metasurfaces that use oligomers as building blocks, it is crucial to be able to solve direct and inverse problems of describing of the QNMs that appear in a given oligomer and to synthesize an oligomer design that supports a certain set of QNMs. To achieve that, a reliable analytical or semianalytical method for analyzing the QNMs of oligomers is necessary. A number of methods that allow studying the optical response of oligomers are available. The multiple-scattering theory [20–26], also known as the coupled-multipole method, allows analytical calculation of the optical response to arbitrary excitation but is not readily usable for finding the QNMs. Full-wave simulations allow studying both scattering and QNMs, but they require the usage of perfectly matched layers that require fine tuning. Moreover, the computational complexity of the simulations increases with the size of the system. There are also analytical methods to study the QNMs of a particle of arbitrary shape [27,28], but they are only applicable to trivially connected structures and not to oligomers.

The analysis of mode coupling in optical oligomers is complicated because of different multipoles to be taken into account. Figure 1(a) illustrates that in the region of the dipole Mie resonance the Lorenz-Mie coefficients corresponding to higher multipoles have nonzero values. Account of only dipole-dipole coupling introduces a considerable error in the resonance frequencies and overestimates mode Q factors [see Fig. 1(b)]. Therefore, for studying the QNMs of an optical oligomer, one has to consider higher multipoles as well. The contribution of higher multipoles becomes less significant for high-index materials but is still significant for frequently used dielectric materials such as silicon [29,30]. Also, optical oligomers are characterized by an intricate coupling, which is illustrated by Fig. 1(c)—each multipole in one scatterer couples with all modes in the other one.

As the dipole resonance is the most robust, in practical cases we usually interested only to the spectral region around the dipole resonance of the individual scatterers of the oligomer. Figure 1(a) shows that the contribution of the dipole mode dominates among other higher-order multipoles. Therefore the coupling of the dipole modes to higher multipoles is weak and just a subject of small corrections [see schematic shown in Fig. 1(c)].

In this paper we present an *optical downfolding* method, which allows an efficient procedure for exact finding of dipole-based QNMs of an optical oligomer. The proposed method is based on the multiple-scattering theory considering all significant multipoles in every scatterer. The main idea of the downfolding procedure is shown in Fig. 1(d). The dipole-dipole coupling is treated rigorously, while higher multipoles are downfolded, i.e., treated as a perturbation and introduced afterwards.

*alexey.dmitriev@metalab.ifmo.ru

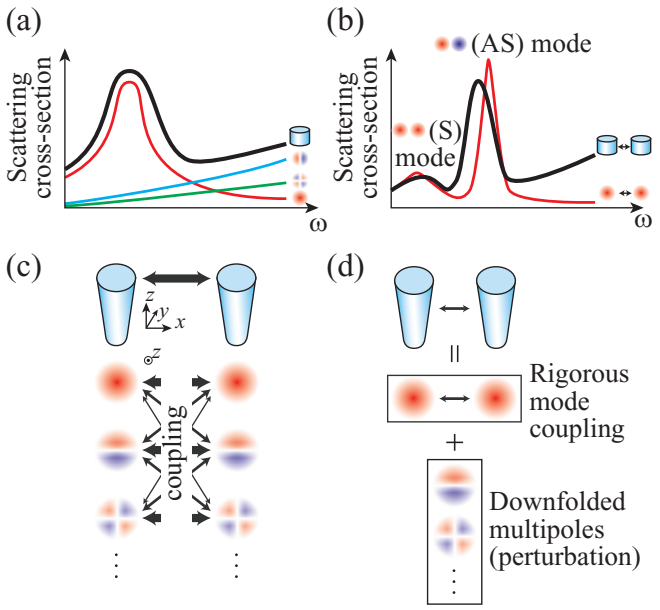

FIG. 1. Schematic representation of the optical downfolding method. (a) Typical scattering spectrum of individual nanopillar around the dipole Mie resonance (thick line); thin curves show the contributions of higher multipoles. (b) Typical scattering spectrum of dimer. Thick curve shows exact spectrum, while the thin curve corresponds to dipole approximation. (c) Diagram revealing coupling of each multipole in one nanopillar with every multipole in the other one. Thicker arrows correspond to stronger coupling. (d) Optical downfolding method consists in treating interaction with the higher multipoles as a perturbation allowing reduction of the problem to the dipole-dipole coupling only.

The paper is organized as follows. First, we briefly review the basics of multiple-scattering theory in Sec. II. After that we describe the optical downfolding (Sec. III). In Sec. IV we demonstrate a detailed analysis of an optical dimer in 2D space. As an illustration, we apply this technique to explain a Fano resonance observed in an optical trimer (Sec. V).

II. MULTIPLE-SCATTERING THEORY

Our approach is based on the coupled-multipole method also known as multiple-scattering theory, which is a semianalytic method allowing fast computation of optical response of optical oligomers [20–26,31–35]. Here we briefly overview this method. For simplicity, we consider here a two-dimensional problem, which allows reducing the problem into two independent polarizations having a leading field that only has one component, which can be treated as scalar. The field is written as a multipole decomposition with azimuthal numbers $l = -N, -N+1, \ldots, N$ around each scatterer. The scattering is described by the Lorentz–Mie coefficients a_l, which link the coefficients of the incident-wave multipole expansion to the corresponding multipole coefficients in the scattered wave. Then we rewrite the field scattered by each of the M scatterers as a multipole expansion in the vicinity of every other scatterer in the system (see Appendix). This procedure yields a system of the algebraic equations which can be written as a single matrix equation. The coupled-multipole matrix A, which consists of $(M \times M)$ blocks of size $([2N+1] \times [2N+1])$, acts on the vector containing the scattered multipole amplitudes. The result is a vector containing the multipole amplitudes of the excitation field. Solving this matrix equation allows us to find the scattered field.

III. QUASI-NORMAL MODES OF A DIMER

In this section we describe our approach to finding the quasinormal modes of an optical oligomer. For simplicity, we demonstrate it on the simplest oligomer that is a dimer. For demonstration we choose the refractive index $n = 4$ (e. g., germanium in the infrared range) and show both TE and TM polarizations. As an oligomer is an open system, that is, it has radiation losses, its QNM frequencies are complex. Here, for simplicity, we introduce a dimensionless complex frequency $x + iy = k'R + ik''R$.

We have to find the null space of the matrix A,

$$A = \left[\begin{array}{c|c} E & V(\mathbf{d}) \\ \hline V(-\mathbf{d}) & E \end{array}\right], \tag{1}$$

where E is an $([2N+1] \times [2N+1])$-sized unit matrix, and $V_{l,m}(\mathbf{d}) = -a_l H^{(1)}_{l-m}(kd) e^{-i(l-m)\varphi(\mathbf{d})}$. We note that the Hankel functions $H^{(1)}_{l-m}(kd)$ of k are quasiperiodic, so there exists an infinite number of QNMs. Moreover, this matrix contains all multipoles up to the azimuthal number N, so its kernel is difficult to find. However, the multipoles of the scatterers are separated spectrally, that is, in the spectral range where one multipole dominates, others usually have a small contribution. Therefore we employ a simplification analogous to the Löwdin downfolding technique [36,37], which comes from magnetism. The main idea is to solve the problem rigorously only for states that are in the spectral range of interest, while treating spectrally separated states as a perturbation. Here we use a similar approach to study QNMs of the optical dimer which come from hybridization of dipole Mie resonances of scatterers—thus we solve the problem rigorously in the dipole approximation while treating higher multipoles as a perturbation.

In the dipole approximation the equation defining the kernel of the coupled-multipole matrix is

$$\begin{vmatrix} 1 & -a_0(x+iy)H_0^{(1)}\left((x+iy)\frac{d}{R}\right) \\ -a_0(x+iy)H_0^{(1)}\left((x+iy)\frac{d}{R}\right) & 1 \end{vmatrix} = 0. \tag{2}$$

As the solutions are supposed to be close to the pole of the Lorenz-Mie coefficient a_0, it is convenient to rewrite this equation as follows:

$$\frac{1}{a_0^2(x+iy)} = \left[H_0^{(1)}\left([x+iy]\frac{d}{R}\right)\right]^2. \tag{3}$$

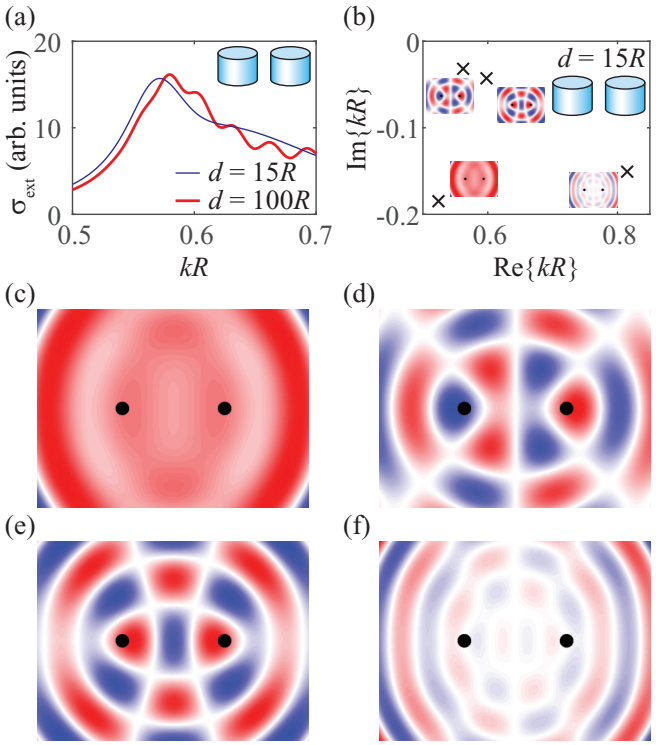

FIG. 2. Quasi-normal modes of germanium nanopillar dimer. (a) Extinction spectra of dimers with distances $d = 100R$ (thick curve) and $d = 15R$ (thin curve). (b) Complex eigenfrequencies of the dimer with distance $d = 15R$. Insets display the corresponding field distributions, which are shown in larger scale in panels (c–f). Refractive index $n = 4$, TE polarization.

We show, for example, the solutions of this equation for a dimer made of germanium ($n = 4$) with $d = 15R$ in the TE polarization in Fig. 2(b). Four complex eigenfrequencies exist in the plotted region. Their corresponding magnetic field distributions are shown in Figs. 2(c)–2(f). We see that multiple modes coexist and increasing frequency corresponds to an increasing number of magnetic field nodes between the rods. For greater distances the number of nodes is much greater, while the field maxima are pinned at the rods. Therefore we further refer to these modes as Fabry-Pérot–like modes.

We plot the left- and right-hand sides of Eq. (2) in the range close to the pole of the Lorenz-Mie coefficient in Fig. 3(a) for $d = 100R$ and Fig. 3(b) for $d = 15R$. As we noted previously, this equation has an countably infinite number of solutions which correspond to quasi–Fabry-Pérot modes and can display a complicated behavior as function of the distance d between the scatterers. In particular, they can form a helical line revolving around the single-cylinder scattering pole in the complex plane [35,38].

However, in the limit of large but finite d this system can be "diagonalized" in the sense of assigning a unique quantum number p to each QNM. To demonstrate this, let us introduce a dimer scaling coefficient $\rho = \frac{d}{R}$ and consider the Hankel function asymptotic at $\rho \to \infty$:

$$H_l^{(1)}(x) \sim \sqrt{\frac{2}{\pi x}} i^{-l} e^{-i\frac{\pi}{4}} e^{ix}. \tag{4}$$

In this case, Eq. (2) can be written as

$$\frac{1}{a_0^2(x+iy)} = \frac{2}{\pi\rho(x+iy)} e^{-2\rho y} e^{2i\rho x}. \tag{5}$$

As is seen from Fig. 3, the function in the left-hand side of the equation has a zero at the point $x_0 + iy_0$ which corresponds to single-cylinder scattering matrix pole. Aside from this zero it is smooth and does not have any sudden phase changes in all the $x > 0$ half-plane. On the contrary, the function at the right-hand side contains a periodic multiplier $e^{2i\rho x}$. Still, it is always possible to choose the scaling parameter ρ to be so large that the left-hand part would remain almost constant on the whole period of the exponential, as is shown in Fig. 3(a). At the same time, as we can see from the $e^{-2\rho y}$ multiplier, large ρ causes the absolute value of the right-hand side to grow very quickly at $y < 0$—therefore all solutions will have

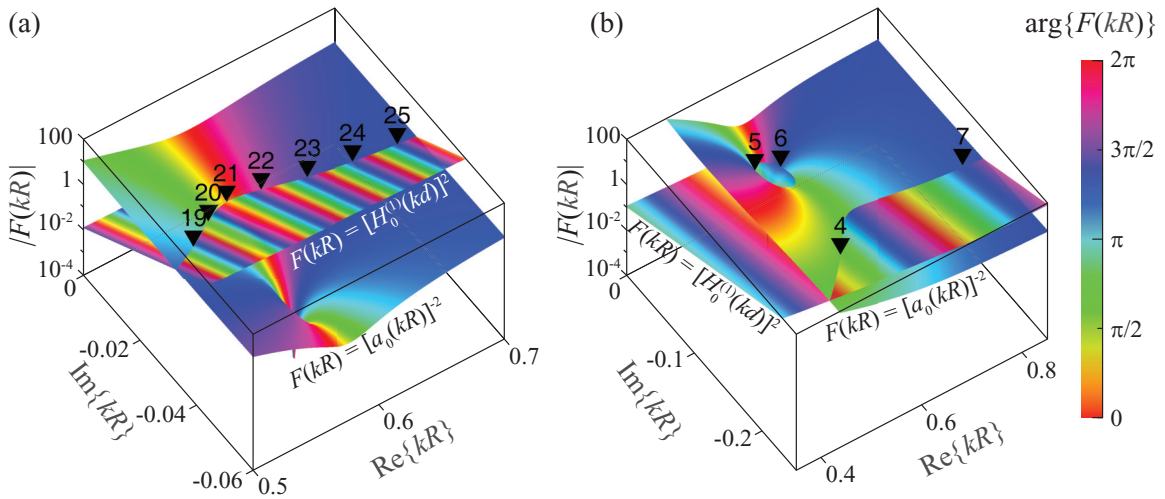

FIG. 3. Graphical solution of Eq. (3). The surfaces show its left- and right-hand sides, as functions of $kR = x + iy$. The z axis corresponds to the absolute values, and the color shows the arguments. Refractive index $n = 4$, TE polarization, $d = 100R$ (a) and $d = 15R$ (b).

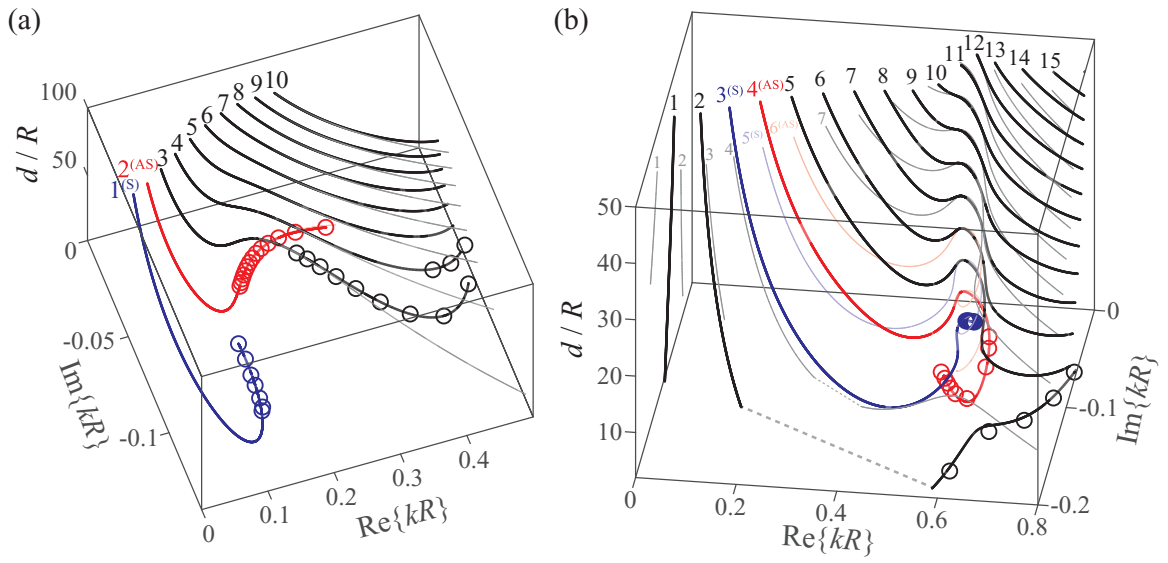

FIG. 4. Quasi-normal mode complex frequencies of germanium nanopillar dimer ($n = 4$) for TM (a) and TE (b) polarizations. The curves demonstrate the results obtained in the dipole approximation ($l_{\max} = 0$, thin lines) and with quadrupoles taken into account ($l_{\max} = 1$, thick lines). Circles show the complex frequencies obtained by full-wave numerical simulations. The symmetric and antisymmetric modes are shown in blue and red color, respectively. The dashed lines connect pieces of the same mode frequency curve cut at $\mathrm{Im}kR = -0.2$.

$y > y_0$ and lie on a single non-self-intersecting curve and can therefore be enumerated.

If we choose a smaller ρ, some QNM frequencies may separate, as is seen in Fig. 3(b), making enumerating them nontrivial. Therefore we diagonalize the system in the large ρ limit and follow the evolution of QNM frequencies with decreasing ρ. After that we introduce higher multipoles as a perturbation using the dipole approximation QNM frequencies as the starting values to search the new solutions around.

In Fig. 4 we show the evolutions of the complex eigenfrequencies $(x + iy)$ as a dependence of ρ for TM and TE polarizations. At large ρ we assign the modes quantum numbers p which are shown as labels next to the curves. As is seen from Fig. 4 and also from Fig. 3(b), at low ρ the eigenfrequencies no longer follow the order existing for large ρ, so the quantum numbers cannot be assigned in a meaningful way by considering only small distances. We note that in the TM polarization case, taking quadrupole modes into consideration only introduces a significant correction for higher frequencies, that is, in the region $x > 0.3$, which corresponds to the quadrupolar Lorenz-Mie coefficient as large as 0.05. Taking even higher multipoles into account only introduces a negligible correction (up to 1%), so we do not show them on the plot. In the TE polarization case, in contrast, the quadrupolar Lorenz-Mie coefficient is not negligible at the frequency of the dipole resonance, so it cannot be downfolded. Instead, we have to solve the problem rigorously by taking the quadrupolar contribution into account, but we still can downfold even higher multipoles. Indeed, as can be seen from Fig. 4(b), the curves obtained by rigorous calculations with dipole only, and dipole and quadrupole taken into account, demonstrate a striking difference in the entire spectral range of interest. We also note the agreement between the computations with the quadrupole taken into account and the full-wave simulations (shown with circles).

IV. EXCEPTIONAL POINTS IN QUASI–FABRY-PÉROT MODES

We note from Fig. 4 that the frequencies of quasi–Fabry-Pérot modes may or may not form a helical line. This kind of helical line may be observed, for example, in the dipole model results (thin lines) in Fig. 4(b). We note that here we will consider TE polarization; however, as our purpose here is not to obtain precise numbers but to demonstrate the physics, we will limit the consideration to the dipole model for simplicity. Here we choose dimers with $n \simeq 5$ for demonstration and consider their modes with quantum numbers $p = 7$ and 9. In Fig. 5(a) we show the trajectories of these eigenfrequencies as dependencies of ρ for a dimer with $n = 4.9$ and in Fig. 5(b) for $n = 5.1$. Both plots here demonstrate a helical line, but there is a change of topology. For $n = 4.9$ the repulsion between the eigenfrequency trajectories is in a horizontal plane, and the mode with $p = 7$ demonstrates a helical line. For $n = 5.1$, in contrast, the helical line is observed for $p = 9$, and the trajectories repulse in a vertical plane. This change of topology corresponds to an exceptional point for the set of parameters (namely, n and ρ) for which these trajectories would touch. To prove this hypothesis, we vary both n and ρ and plot the real and imaginary parts of the eigenfrequencies as a three-dimensional plot. The results are shown in Figs. 5(c) and 5(d). The eigenfrequency surfaces demonstrate a topology characteristic to exceptional points [39] that exhibits a crossing-to-anticrossing transition upon passing an exceptional point. Physically, an exceptional point is a special kind of degeneracy for which not only eigenfrequencies but also field distributions are degenerated. We plot the field distributions near and at the exceptional point in the insets on Fig. 5(a) and 5(b). We note that field distributions corresponding to different modes all resemble the field distribution at the exceptional point (EP). Exceptional points are usually considered in optical systems consisting of coupled resonators

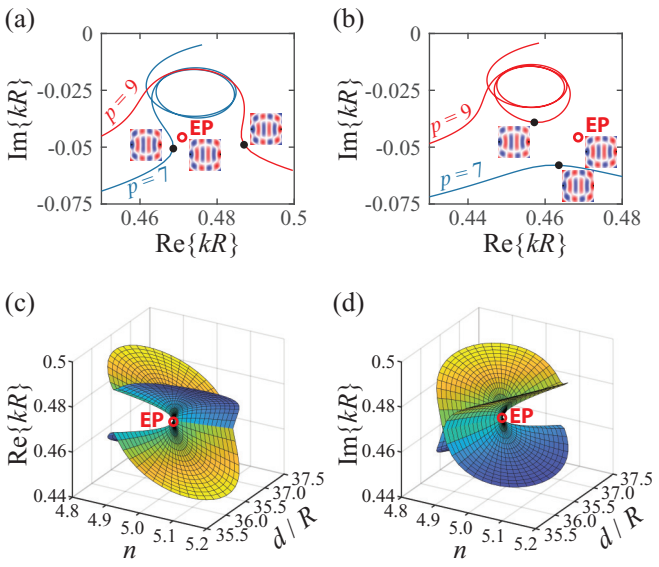

FIG. 5. Complex frequencies of the quasinormal modes of dimer for the distance d varied continuously. The curves correspond to the mode quantum numbers $p = 7$ (blue) and $p = 9$ (red) for dimer refractive indices $n = 4.9$ (a) and $n = 5.1$ (b). The minimum distances between mode frequencies occur for $d = 35.8R$ in plot (a) and for $d = 37.1R$ for plot (b) and are marked by black dots. Insets show the mode field distributions at the corresponding frequencies. The plots in (c,d) show real (c) and imaginary (d) parts of $p = 7$ and 9 mode frequencies as two-dimensional functions of refractive index n and normalized distance d/R. TE polarization, dipole approximation.

with gain and loss, or with different amount of loss [39,40]. For example, an EP in a PT-symmetric dimer with gain and loss has also been reported in Ref. [41]. However, in our case there is no loss contrast: the nanopillars are equivalent and have no loss other than radiative. Nevertheless, there still are certain parameters that correspond to mode degeneration, i.e., exceptional points.

V. EIGENFREQUENCIES OF A TRIMER EXHIBITING FANO RESONANCE

Here we apply the optical downfolding method to a trimer. For simplicity, we only briefly describe the modifications that have to be made to the dimer case here. First, we note that instead of the single distance d, in the case of trimer we have three distances r_{12}, r_{23}, and r_{31}. Nevertheless, we can still introduce a scaling parameter ρ by multiplying these distances by this parameter (in a sense, we apply a scale transformation). After that we apply the Hankel function asymptotic at large ρ to the equation $\det A = 0$, which now has three periodic parts with different periods that depend on r_{12}, r_{23}, and r_{31}.

Now we consider a linear trimer of rods of radius R made of a material with refractive index $n = 4$. The distance between the centers of neighbor rods is $5R$. We consider TM polarization. We plot the extinction spectrum obtained by the coupled-multipole method in Fig. 6(a). The spectrum shows that the dipole peak is split into 3. Moreover, there is a dip

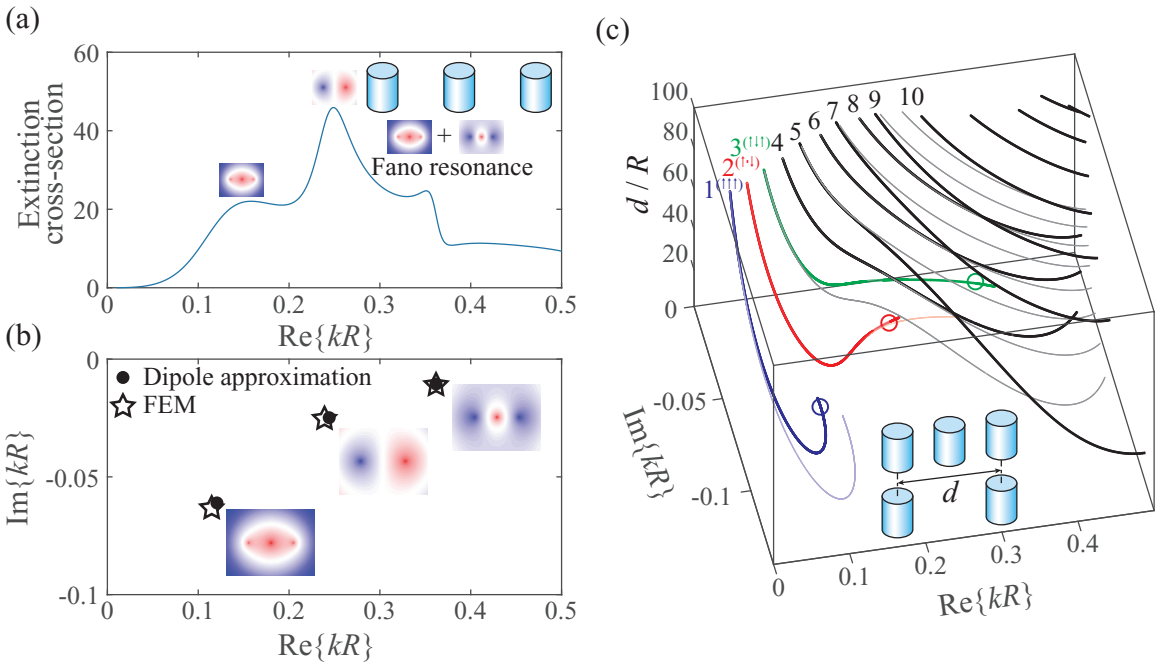

FIG. 6. Quasi-normal modes of germanium nanorod linear trimer. Refractive index $n = 4$, TM polarization. Distance between the centers of neighbor rods is $2.3R$. (a) Extinction spectrum of the trimer. (b) Complex frequencies of the trimer quasinormal modes. Symbols show the results obtained in dipole approximation (circles) and using full-wave numerical simulations (stars). Insets show the mode field distributions. (c) Quasi-normal mode complex frequencies of germanium nanopillar trimer (thick lines) and dimer (thin lines). The frequencies were calculated with quadrupoles taken into account ($l_{\max} = 1$). Circles indicate the frequencies shown at panel (b). The symmetric (↑↑↑), second symmetric (↑↓↑), and antisymmetric (↑ 0 ↓) modes are shown in blue, green, and red colors, respectively. The inset shows our choice of scaling distance d.

near the third peak, which suggests that a Fano resonance may be present in the trimer.

In order to interpret these peaks, we find the corresponding QNMs with the approach described before. As is seen from Fig. 6(b), the lowest peak corresponds to the first symmetric mode (↑↑↑). The middle peak corresponds to the asymmetric mode (↓ 0 ↑). The highest peak corresponds to the second symmetric mode (↓↑↓). We also note that the corresponding QNM has the highest quality factor, five times higher than that of the (↑↑↑) mode.

Let us now discuss the necessary conditions for the Fano resonance to appear in the scattering spectrum. By considering the far-field pattern of the scattered field, it is straightforward to show that the forward-scattering amplitude, which determines the extinction cross section, reads

$$F(0) = \sum_j e^{-i\vec{k}_i\cdot\vec{r}_j} \sum_{l=-l_{\max}}^{l_{\max}} i^{-l} e^{-i\frac{\pi}{4}} a_{jl}, \tag{6}$$

where the index j runs over all scatterers. For simplicity, let us rewrite this expression for a dimer in the dipole approximation:

$$F(0) = \langle e^{i\vec{k}\cdot\vec{r}}|a\rangle, \quad |e^{i\vec{k}\cdot\vec{r}}\rangle = \begin{bmatrix} e^{i\vec{k}\cdot\vec{r}_1} \\ e^{i\vec{k}\cdot\vec{r}_2} \end{bmatrix}, \quad |a\rangle = \begin{bmatrix} a_{10} \\ a_{20} \end{bmatrix}. \tag{7}$$

That is, forward-scattering amplitude is equal to the inner product of the vector of scattering amplitudes $|a\rangle$ with the incident plane wave $|e^{i\vec{k}_i\cdot\vec{r}}\rangle$ at the centers of the scatterers $\vec{r} = \vec{r}_j$. We note that the incident plane wave, which has a real frequency, excites a set of quasinormal modes of the system:

$$|a\rangle = \sum_q A_q |\mathrm{QNM}_q\rangle. \tag{8}$$

In other words, the response a_{jl} that can be decomposed into a linear composition of the QNMs. The incident plane wave $e^{i\vec{k}_i\cdot\vec{r}}$ can be written in the basis of the QNMs too:

$$|e^{i\vec{k}\cdot\vec{r}}\rangle = \sum_{q'} B_{q'} |\mathrm{QNM}_{q'}\rangle. \tag{9}$$

We now note from Eq. (7) that interference terms $A_q B^*_{q'} \langle \mathrm{QNM}_{q'}|\mathrm{QNM}_q\rangle$ leading to Fano resonance [42] may appear in the forward-scattering amplitude if the quasinormal modes q and q' are not orthogonal to each other.

We now use the calculated complex frequencies to find the null-space basis vectors $|\mathrm{QNM}_q\rangle$ of the coupled-multipole matrix A. We find that the vector corresponding to the antisymmetric mode is orthogonal to both symmetric modes, while first and second symmetric modes are not orthogonal to each other and may couple. Therefore the Fano resonance is attributed to the interaction of the (↑↑↑) mode acting as a continuum and the (↓↑↓) mode acting as a discrete state.

Let us now discuss the evolution of the eigenmode frequencies of a trimer shown in Fig. 6(c). As is seen from the figure, the antisymmetric modes, which correspond to the odd quantum numbers p, do not demonstrate a significant difference until very close spacings between the nanopillars. This is explained by the fact that the antisymmetric modes have a zero field in the oligomer center; therefore the presence of a third nanopillar in the middle does not significantly influence the mode field distribution. The symmetric modes corresponding to even p, in contrast, demonstrate a considerable difference between the dimer and the trimer. First the lowest symmetric mode (↑↑↑) has a smaller Q factor for a trimer than for a dimer. Another difference is that the second symmetric mode (↑↓↑) in the case of a dimer is a Fabry-Pérot–like mode with the center field maximum in air. Therefore, its Q factor becomes far greater in the trimer case, where the central field maximum is pinned inside a nanopillar, as compared to the dimer. The higher Fabry-Pérot–like modes, in contrast, do not demonstrate a significant difference between the dimer and trimer cases.

VI. CONCLUSION

To summarize, we have studied optical mode coupling in a dimer and a linear trimer of nanopillars in the spectral region around the dipole Mie resonance of an individual nanopillar. In our studies we used an originally developed *optical downfolding* technique based on the multiple-scattering theory, which consists of a rigorous consideration of the dipole-dipole coupling and introducing downfolded higher multipoles afterwards, treating the latter as a perturbation. The proposed method works at arbitrary distances between the nanopillars. This technique allowed us to analyze the quasinormal modes of a dimer and to reveal the physical nature of the Fabry-Pérot–like modes that exhibit approximately equidistant fringes in the scattering spectra. We have also demonstrated that these modes can coalesce to exceptional points at certain sets of dimer parameters. The special crossing-to-anticrossing topology of these exceptional points have been demonstrated to determine the behavior of eigenfrequencies with changing distance between the nanopillar—whether they repulse along the real or the imaginary parts. Using our technique to study the modes of a linear trimer helped to find which quasinormal modes interact, with the result that they appear as a Fano resonance in the trimer scattering spectrum. Our predictions agree well with the finite-element-method simulations for systems small enough for the latter to be applicable. The proposed method can also be applied to arbitrary oligomers.

ACKNOWLEDGEMENT

We acknowledge a support from the Russian Science Foundation (Grant No. 21-72-30018).

APPENDIX: MULTIPLE-SCATTERING THEORY

Considering each polarization separately and assuming time harmonics of the form $\exp(-i\omega t)$, we denote the leading field component as a scalar field ψ and solve the problem in the frequency domain. We also restrict our consideration to the case of all scatterers to be similar. This simplifies the analysis, while also being a reasonable assumption, as in reality it is easier to fabricate arrays of particles of the same size rather than to vary it [8–10]. To demonstrate the physics, here we choose the simplest shape, which is a circle, or, equivalently, an infinite cylinder.

We use a multipole expansion at the center of each scatterer, so we can write the incident $\psi_i^{(j)}$ and the scattered $\psi_s^{(j)}$ waves in the vicinity of the jth scatterer as

$$\psi_i^{(j)}(\mathbf{r}) = \psi_{\text{ext}} + \sum_{l=-N}^{N} I_{j,l} J_l(k|\mathbf{r}-\mathbf{r}_j|) e^{-il\varphi(\mathbf{r}-\mathbf{r}_j)},$$
$$\psi_s^{(j)}(\mathbf{r}) = \sum_{l=-N}^{N} S_{j,l} H_l^{(1)}(k|\mathbf{r}-\mathbf{r}_j|) e^{-il\varphi(\mathbf{r}-\mathbf{r}_j)}, \tag{A1}$$

where $\varphi(\mathbf{r})$ denotes the angle of the vector $\mathbf{r}$ in polar coordinates, k is the wave number, and $\mathbf{r}_j$ is the rod position. $H_l^{(1)}$ is the Hankel function related to the outgoing waves, J_l is the Bessel function related to the incident waves, N is the maximal azimuthal number of multipoles under consideration, and ψ_{ext} is the excitation field, i.e., the waves from external sources. Scattering is described by the Lorenz-Mie coefficients:

$$S_{j,l} = a_l I_{j,l}, \tag{A2}$$

where a_l is the Lorenz-Mie coefficient for the lth multipole. Each scatterer is described by the same set of Lorenz-Mie coefficients:

$$a_l(n,\xi) = \frac{\nu J_l(\xi) J_l'(\xi) - J_l'(\xi) J_l(n\xi)}{\left(H_l^{(1)}(\xi)\right)'(\xi) J_l(n\xi) - \nu H_l^{(1)}(\xi) J_l'(\xi)}, \tag{A3}$$

where $\nu = n$ in case of the TM polarization (the magnetic field is orthogonal to the cylinder axis and the electric field oscillates along it) and $\nu = -1/n$ in case of the TE polarization (the magnetic field oscillates along the axis), $\xi = R\omega/c$ is the size parameter, and n and R are the refractive index and radius of the cylinder.

Next we note that the field, which is incident to jth rod, consists of the excitation and the sum of the fields scattered by each of the other rods. By means of the addition theorem it is straightforward to show that

$$I_{j,l} = \sum_{i\neq j} \sum_{m=-N}^{+N} H_{l-m}^{(1)}(kr_{ij}) e^{-i(l-m)\varphi(\mathbf{r}_{ij})} S_{i,m}, \tag{A4}$$

where $\mathbf{r}_{ij} = \mathbf{r}_i - \mathbf{r}_j$.

Using Eqs. (A2) and (A4) together, we express either $I_{j,l}$ or $S_{j,l}$ (here we choose the latter) to obtain a system of $([2N+1]\times M)$ algebraic equations with the same number of unknowns. Here M is the number of rods.

The system of the algebraic equations obtained from combining Eqs. (A2) and (A4) can be written as a single matrix equation. The coupled-multipole matrix A, which consists of $(M\times M)$ blocks of size $([2N+1]\times[2N+1])$, acts on the vector containing the scattered multipole amplitudes $S_{j,l}$. The result is a vector containing the multipole amplitudes of the excitation field. It is straightforward to show that the matrix equation for the case of two rods can be expressed as

$$\sum_{j,m} A_{im,jl} S_{j,l} = a_m X_{i,m}, \tag{A5}$$

where X is the vector of excitation field multipoles (for a plane wave it can be obtained with the Jacobi-Anger expansion) and

$$A_{im,jl} = \delta_{ij}\delta_{lm} - [1-\delta_{ij}] a_l H_{l,m}^{(1)}(kr_{ij}) e^{-i(l-m)\varphi(\mathbf{r}_{ij})}. \tag{A6}$$

The inverse coupled-multipole matrix A^{-1} being an analog of a Green function allows us to solve the electrodynamic problem: its inner product with the excitation vector yields the multipole amplitudes of the scattered field ($S = A^{-1}X$), which can be used to calculate the extinction cross section σ_{ext} in a straightforward way (see, e. g., [35]).

To provide an example, we show in Fig. 2(a) the TE polarization extinction spectra of dimers made of germanium ($n = 4$) with the distance d between the centers of the rods being 25 and 100 times larger than the radius. The spectra exhibit a dipole Mie resonance at $kR = 0.58$ and fringes associated with Fabry-Pérot–like modes which are discussed later. The spectrum for $d = 100R$ shows a large number of clearly evident fringes which correspond to Fabry-Pérot modes. In contrast, for $d = 25R$ only two fringes can be clearly distinguished in the spectrum, which correspond to a small number of modes with large negative imaginary parts of the corresponding eigenfrequencies.

Here we are interested in the quasinormal modes of the system of scatterers—that is, nontrivial optical states (which may be damping) that can exist without any excitation. They correspond to the kernel (null space) of the coupled-multipole matrix A. Like in an eigenvalue problem, we first find the QNM frequencies ω defined by the equation $\det A(\omega) = 0$ and then use them to solve a homogeneous matrix equation $A(\omega)S = 0$ to find the corresponding vectors S.

We note that in the dipole approximation with Lorentzian response, $A = (\mathscr{H} - \omega E)$, where $\mathscr{H}$ is the effective Hamiltonian and E is a unit matrix [35]. Therefore the quasinormal modes can be written in this approximation as $\ker(\mathscr{H} - \omega E)$, i.e., they are the eigenvectors of the system.

[1] W. T. Chen, A. Y. Zhu, and F. Capasso, Flat optics with dispersion-engineered metasurfaces, Nat. Rev. Mater. **5**, 604 (2020).

[2] Q. He, S. Sun, S. Xiao, and L. Zhou, High-efficiency metasurfaces: Principles, realizations, and applications, Adv. Opt. Mater. **6**, 1800415 (2018).

[3] J. Sung, G.-Y. Lee, and B. Lee, Progresses in the practical metasurface for holography and lens, Nanophotonics **8**, 1701 (2019).

[4] M. L. Tseng, H.-H. Hsiao, C. H. Chu, M. K. Chen, G. Sun, A.-Q. Liu, and D. P. Tsai, Metalenses: Advances and applications, Adv. Opt. Mater. **6**, 1800554 (2018).

[5] B. Yang, H. Cheng, S. Chen, and J. Tian, Structural colors in metasurfaces: Principle, design and applications, Mater. Chem. Front. **3**, 750 (2019).

[6] Z. H. Jiang, S. Yun, L. Lin, J. A. Bossard, D. H. Werner, and T. S. Mayer, Tailoring dispersion for broadband low-loss optical

metamaterials using deep-subwavelength inclusions, Sci. Rep. **3**, 1571 (2013).

[7] X. Wang, Z. Nie, Y. Liang, J. Wang, T. Li, and B. Jia, Recent advances on optical vortex generation, Nanophotonics **7**, 1533 (2018).

[8] V.-C. Su, C. H. Chu, G. Sun, and D. P. Tsai, Advances in optical metasurfaces: Fabrication and applications [invited], Opt. Express **26**, 13148 (2018).

[9] S. Walia, C. M. Shah, P. Gutruf, H. Nili, D. R. Chowdhury, W. Withayachumnankul, M. Bhaskaran, and S. Sriram, Flexible metasurfaces and metamaterials: A review of materials and fabrication processes at micro- and nano-scales, Appl. Phys. Rev. **2**, 011303 (2015).

[10] U. Zywietz, A. B. Evlyukhin, C. Reinhardt, and B. N. Chichkov, Laser printing of silicon nanoparticles with resonant optical electric and magnetic responses, Nat. Commun. **5**, 3402 (2014).

[11] H. Wang, D. W. Brandl, P. Nordlander, and N. J. Halas, Plasmonic nanostructures: Artificial molecules, Acc. Chem. Res. **40**, 53 (2007).

[12] J. H. Yan, P. Liu, Z. Y. Lin, H. Wang, H. J. Chen, C. X. Wang, and G. W. Yang, Magnetically induced forward scattering at visible wavelengths in silicon nanosphere oligomers, Nat. Commun. **6**, 7042 (2015).

[13] P. Alonso-Gonzalez, M. Schnell, P. Sarriugarte, H. Sobhani, C. Wu, N. Arju, A. Khanikaev, F. Golmar, P. Albella, L. Arzubiaga, F. Casanova, L. E. Hueso, P. Nordlander, G. Shvets, and R. Hillenbrand, Real-space mapping of Fano interference in plasmonic metamolecules, Nano Lett. **11**, 3922 (2011).

[14] *Reviews in Plasmonics 2015*, edited by C. D. Geddes (Springer International Publishing, Cham, Switzerland, 2016).

[15] G. Haran and L. Chuntonov, Artificial plasmonic molecules and their interaction with real molecules, Chem. Rev. **118**, 5539 (2018).

[16] N. J. Greybush, I. Liberal, L. Malassis, J. M. Kikkawa, N. Engheta, C. B. Murray, and C. R. Kagan, Plasmon resonances in self-assembled two-dimensional Au nanocrystal metamolecules, ACS Nano **11**, 2917 (2017).

[17] L. Cao, P. Fan, and M. L. Brongersma, Optical coupling of deep-subwavelength semiconductor nanowires, Nano Lett. **11**, 1463 (2011).

[18] T. Shibanuma, S. A. Maier, and P. Albella, Polarization control of high transmission/reflection switching by all-dielectric metasurfaces, Appl. Phys. Lett. **112**, 063103 (2018).

[19] U. Zywietz, M. K. Schmidt, A. B. Evlyukhin, C. Reinhardt, J. Aizpurua, and B. N. Chichkov, Electromagnetic resonances of silicon nanoparticle dimers in the visible, ACS Photon. **2**, 913 (2015).

[20] P. Lloyd and P. Smith, Multiple scattering theory in condensed materials, Adv. Phys. **21**, 69 (1972).

[21] K. M. Leung and Y. Qiu, Multiple-scattering calculation of the two-dimensional photonic band structure, Phys. Rev. B **48**, 7767 (1993).

[22] D. Felbacq, G. Tayeb, and D. Maystre, Scattering by a random set of parallel cylinders, JOSA A **11**, 2526 (1994).

[23] N. A. Nicorovici, R. C. McPhedran, and L. C. Botten, Photonic band gaps for arrays of perfectly conducting cylinders, Phys. Rev. E **52**, 1135 (1995).

[24] G. Tayeb and S. Enoch, Combined fictitious-sources-scattering-matrix method, JOSA A **21**, 1417 (2004).

[25] P. Markoš, Photonic crystal with left-handed components, Opt. Commun. **361**, 65 (2016).

[26] P. Markoš and V. Kuzmiak, Coupling between Fano and Bragg bands in the photonic band structure of two-dimensional metallic photonic structures, Phys. Rev. A **94**, 033845 (2016).

[27] P. Y. Chen, D. J. Bergman, and Y. Sivan, Generalizing normal mode expansion of electromagnetic Green's tensor to open systems, Phys. Rev. Appl. **11**, 044018 (2019).

[28] W. Yan, P. Lalanne, and M. Qiu, Shape Deformation of Nanoresonator: A Quasinormal-Mode Perturbation Theory, Phys. Rev. Lett. **125**, 013901 (2020).

[29] J. P. Barton, D. R. Alexander, and S. A. Schaub, Theoretical determination of net radiation force and torque for a spherical particle illuminated by a focused laser beam, J. Appl. Phys. **66**, 4594 (1989).

[30] A. A. Dmitriev and M. V. Rybin, Optical coupling of overlapping nanopillars, Opt. Lett. **46**, 1221 (2021).

[31] V. Twersky, On a multiple scattering theory of the finite grating and the Wood anomalies, J. Appl. Phys. **23**, 1099 (1952).

[32] G. O. Olaofe, Scattering by two cylinders, Radio Sci. **5**, 1351 (1970).

[33] J. W. Young and J. C. Bertrand, Multiple scattering by two cylinders, J. Acoust. Soc. Am. **58**, 1190 (1975).

[34] T.-G. Tsuei and P. W. Barber, Multiple scattering by two parallel dielectric cylinders, Appl. Opt. **27**, 3375 (1988).

[35] A. A. Dmitriev and M. V. Rybin, Combining isolated scatterers into a dimer by strong optical coupling, Phys. Rev. A **99**, 063837 (2019).

[36] P.-O. Löwdin, A note on the quantum-mechanical perturbation theory, J. Chem. Phys. **19**, 1396 (1951).

[37] O. K. Andersen and T. Saha-Dasgupta, Muffin-tin orbitals of arbitrary order, Phys. Rev. B **62**, R16219 (2000).

[38] E. N. Bulgakov, K. N. Pichugin, and A. F. Sadreev, Evolution of the resonances of two parallel dielectric cylinders with distance between them, Phys. Rev. A **100**, 043806 (2019).

[39] Ş. K. Özdemir, S. Rotter, F. Nori, and L. Yang, Parity-time symmetry and exceptional points in photonics, Nat. Mater. **18**, 783 (2019).

[40] Y. Huang, Y. Shen, and G. Veronis, Non-PT-symmetric two-layer cylindrical waveguide for exceptional-point-enhanced optical devices, Opt. Express **27**, 37494 (2019).

[41] A. Abdrabou and Y. Y. Lu, Exceptional points for resonant states on parallel circular dielectric cylinders, J. Opt. Soc. Am. B **36**, 1659 (2019).

[42] M. F. Limonov, M. V. Rybin, A. N. Poddubny, and Y. S. Kivshar, Fano resonances in photonics, Nat. Photon. **11**, 543 (2017).